Measurement of the Lidar Ratio for Atmospheric Aerosols using a 180°-Backscatter Nephelometer

Doherty, Sarah J.

Department of Atmospheric Sciences, University of Washington, Box 351640, Seattle, WA 98195-1640

Anderson, Theodore L.

Joint Institute for the Study of the Atmosphere and Oceans, University of Washington, Box 351640, Seattle, WA 98195-1640

Charlson, Robert J.

Department of Atmospheric Sciences, University of Washington, Box 351640, Seattle, WA 98195-1640

Applied Optics: Lasers, Photonics, and Environmental Optics

Doherty, S.J., T.L. Anderson, and R.J. Charlson, Measurement of the lidar ratio for atmospheric aerosols with a 180degree backscatter nephelometer, Applied Optics, 38(9), 20 March 1999, 1823-1832.

Abstract:

Laser radar (lidar) can be used to estimate atmospheric extinction coefficients due to aerosols if the ratio between optical extinction and 180° backscatter (the "lidar ratio") at the laser wavelength is known or if Raman or high spectral resolution (HSR) data is available. Most lidar instruments do not have Raman or HSR capability, however, making knowledge of the lidar ratio essential. We have modified an integrating nephelometer, which measures the scattering component of light extinction, by addition of a backward pointing laser light source such that the detected light corresponds to integrated scattering over 176°-178° at a common lidar wavelength of 532 nm. Mie calculations indicate that the detected quantity is an excellent proxy for 180° backscatter. When combined with existing techniques for measuring total scattering and absorption by particles, the new device permits a direct determination of the lidar ratio. A four-point calibration, run by filling the enclosed sample volume with particle-free gases of known scattering coefficient, indicates a linear response and calibration reproducibility to within 4%. The instrument has a detection limit of 1.5×10^{-7} m^{-1} sr^{-1} (~10% of Rayleigh scattering by air at STP) for a 5 minute average, and is suitable for ground and mobile/airborne surveys. Initial field measurements yielded a lidar ratio of ~20 for marine aerosols and ~60-70 for continental aerosols, with an uncertainty of ~20%.

Key words: lidar ratio, nephelometer, backscatter, climate forcing, aerosol, light scattering

1.0 Introduction

A recent National Research Council panel report[1] summarizes six independent lines of evidence supporting the hypothesis that direct (i.e. clear-sky) climate forcing due to the scattering and absorption of sunlight by anthropogenic aerosols is a major factor in global climate change. Visibility is similarly known to depend on scattering and absorption of light by atmospheric aerosols. A variety of aerosol measurements (as well as theoretical models) contribute to this evidence, but notably lacking is a physically meaningful contribution from elastically scattering lidar. Nevertheless, the *potential* contribution of this technology is enormous, given its exquisite precision, vertical resolution, and the relative ease of data acquisition. This potential has yet to be exploited because of difficulties in quantitatively and accurately relating the elastically scattered lidar signal to the aerosol parameters relevant to climate forcing and visibility.

Analogous to radar but operating at shorter wavelengths, a lidar instrument transmits pulsed laser radiation and measures what is backscattered by gases, particles, or other objects in the atmosphere. The return time of the signal corresponds to distance from the transmitter such that range-dependent information is acquired. The intensity of the signal depends on two quantities: (1) how effectively the laser radiation is backscattered at a specific location in the atmosphere and (2) how effectively the laser radiation is extinguished by the intervening atmosphere. Interpreting the lidar signal depends on an ability to separate these two quantities - local 180° backscatter and optical depth over the entire range. It is this deconvolution of local backscatter and range-dependent optical depth which is at the heart of the lidar retrieval challenge.

Following instrument calibration[2], a vertically-pointing lidar provides a direct measurement of the quantity S(z):

$$S(z) = A\beta(z)\exp[-2\int_{z_L}^{z} \sigma_e(z')dz] = A\beta(z)\exp[-2\tau(z_L,z)] \qquad (1)$$

where A is an instrumental calibration constant, $\beta(z)$ is the 180° backscatter coefficient (m^{-1} sr^{-1}) from both molecules and aerosols at height z (m), σ_e is the extinction coefficient (m^{-1}) from both

molecules and aerosols at height z, and $\tau(z_L,z)$ is the extinction optical depth between the lidar height, z_L, and z. Eq. 1 shows that the fundamental challenge of converting the lidar measurement, S(z), to a geophysically meaningful aerosol quantity is to disentangle β and τ - or, equivalently, β and σ_e. Since molecular scattering can be predicted accurately from air density (i.e. temperature and pressure) information, this challenge reduces to disentangling particulate backscattering, β_p, from particulate extinction, σ_{ep}. Two types of technologically advanced lidar systems, Raman lidar and high spectral resolution lidar, are able to separate these terms by making auxiliary measurements of the return signal. These instruments are described briefly in Section 4.

For lidar systems that detect elastically scattered light only, the quantities β_p and σ_{ep} can be disentangled if the ratio of the two parameters is known. This quantity is referred to as the lidar ratio[3], K,

$$K(sr) = \frac{\sigma_{ep}}{\beta_p} = \frac{\sigma_{sp} + \sigma_{ap}}{\beta_p} \qquad (2)$$

where σ_{sp} and σ_{ap} are the components of particulate extinction due to light scattering and light absorption, respectively.

Based on Mie calculations that incorporate the ranges of particle size distributions and refractive indices encountered in the troposphere, possible values of K span at least an order of magnitude, from approximately 10 to 100 (sr). The lower values correspond to coarse-particle aerosols like soil dust and sea salt, while the higher values represent fine particles of smoke and products of gas-to-particle conversion. To explore the sensitivity of lidar-retrieved optical depth to uncertainties in K, we use data from the recent lidar demonstration Shuttle mission[4] (LITE). Table 1 shows the effect on retrieved optical depth of allowing K to vary from 10 to 100. Data consists of two cases when aerosol layers were detected at night over Africa during the LITE mission. The columns labeled $?\log\tau_p/?\log K$ indicate how a fractional uncertainty in lidar ratio would translate into a fractional uncertainty in optical depth. This sensitivity parameter is seen to vary between the two cases and to be a strong function of lidar ratio. For low K values, K and τ_p are nearly proportional. For the higher K values (which tend to be characteristic of pollution-

derived particles in the sub-μm size range), the sensitivity is considerably higher - up to a factor of 4. Overall, the factor of ten range of possible lidar ratios translates into a factor of 10 to 40 uncertainty in retrieved optical depth. This range is too large to offer an adequate constraint on lidar retrievals for the problems of climate forcing or visibility.

For lack of accurate knowledge of K, most aerosol measurements by elastically scattered lidar are reported as a "scattering ratio" - that is, the ratio of the calibrated signal to the expected signal for particle-free air.[5-12]. This is useful for qualitative identification of aerosol layers, but not for input into radiative transfer models. The instrument described herein provides a relatively inexpensive method for accurate local measurement of β_p. When combined with existing instrumentation for measuring σ_{ep}, this permits an empirical determination of K.

Being small and portable, the new device permits routine ground-based monitoring as well as airborne surveys of β_p and K, which will, in turn, allow extensive lidar data sets on tropospheric aerosols to be applied in a quantitative fashion to the aerosol/climate and visibility problems.

2.0 Design Details

Two technical developments combined to make the 180° nephelometer feasible. First is the commercial development and laboratory validation[13] of a high-sensitivity integrating nephelometer (TSI, Inc., St. Paul, MN). This instrument performs a geometrical integration of the angular distribution of scattered intensity such that the scattering coefficient of a gaseous or aerosol medium can be measured with the combination of a Lambertian light source and an orthogonal light detector. Two versions of the nephelometer are currently available: the 3551, which measures light scattering at one wavelength (550nm) and the 3563, which measures scattering at three wavelengths (450, 550, and 750nm). The instrument already incorporates several key design features needed for accurate measurement of β_p.

1) The scattering volume is enclosed, allowing calibration with gases of known scattering coefficient. Scattering by particle-free air can be measured and

subtracted from subsequent measurements of air containing aerosol to derive light scattering due to particles only, σ_{sp}.

2) A reference chopper is used to alternate between measurement of dark counts, the scattering signal, and a reference signal. The system signal thus is corrected for dark count, changes in lamp brightness, and changes in photomultiplier tube sensitivity using the dark and reference signals.

3) The temperature and pressure within the sensing volume are continuously monitored, so the amount of scattering coming from air within the sensing volume can be accurately calculated and subtracted from total scattering to determine scattering due to particles only (σ_{sp}).

The second technological development of import is the commercial production of a diode-pumped laser operating at 532nm (Uniphase 10mW Microgreen laser). This laser is more compact and stable than gas lasers operating at similar wavelengths and can be incorporated into the TSI nephelometer to provide an alternate, single-beam source of illumination.

Figure 1 schematically shows how a basic version of the integrating nephelometer (model 3551) has been modified to measure near-180° backscatter. The laser and associated optics are added to produce a collimated beam of light that is aimed very nearly along the optical axis of the nephelometer sample volume, pointing away from the detector. With this arrangement, light reaching the detector has either been scattered at near-180° by molecules and particles in the sample volume or it has been scattered off the interior walls. Variations in the laser intensity and detector sensitivity are continuously monitored via a reference beam (Figure 2). Mie calculations show that the 176°-178° scattering integral actually sensed by the nephelometer is an excellent proxy for 180° backscatter for a broad range of particle size distributions and refractive indices (Figure 3). Periodic calibration with gases determines wall scattering (to be subtracted) and the factor that converts the remaining signal to β.

As designed, the system can be run both as a 180° nephelometer, using the laser as the light source, or as a normal nephelometer, using the built-in tungsten-halogen lamp. Ideally, electronically controlled shutters would be integrated into the system for rapid, automatic switching between the two modes, although manual switching between light sources is possible with the current design. In either case, for a valid comparison of total scatter to 180°-backscatter an assumption would need to be made about the stability of the sampled aerosol with time. For the field data presented herein (Section 5), the three quantities needed to determine K (σ_{sp}, β_p, and σ_{ap}) were measured simultaneously with separate instruments.

3.0 Gas calibration & noise measurements

As a closed-volume device, the 180° nephelometer is calibrated with gases of known backscattering coefficient. These absolute calibrations can be performed routinely in the field to maintain a record of calibration stability and an analysis of instrumental noise. In this way, detection limits are quantified and performance is continuously monitored. The system can also be calibrated with monodisperse, laboratory generated particles, where the measured 180° backscatter would be compared to calculated values using Mie theory, as has been done for the integrating nephelometer[13].

The basic algorithm for deriving β_p from the measured photon counts is:

$$\beta_p = k_2(C - C_{wall}) - \beta_{air}(T,P) \tag{3}$$

where k_2 is the calibration slope, C (the instrument signal) is the normalized photon counting rate measured by photo-multiplier tube (PMT), C_{wall} is the calibration offset, which can be interpreted as photon counts associated with scattering off the inside walls, and β_{air} is the calculated 180° backscatter coefficient of air at the temperature (T) and pressure (P) measured inside the instrument. The normalized photon counts, C, are corrected for dark counts (C_{dark}) and variations in laser brightness and PMT sensitivity (via changes in C_{cal}):

$$C = \frac{(C_{meas} - C_{dark})}{(C_{cal} - C_{dark})} \tag{4}$$

A rotating shutter alternately exposes the PMT to backscattered photons, no photons, and a small portion of the laser beam itself to determine C_{meas}, C_{dark}, and C_{cal}, respectively.

The backscattering coefficient of the calibration gases is known to be a function of the refractive index and the molecular anisotropy of the gas[14,15] as follows:

$$\beta_{gas}(\lambda) = \sigma_{sg}(STP,\lambda)\frac{3}{8\pi}\frac{(1+\gamma)}{(1+2\gamma)}\frac{273.2}{T}\frac{P}{1013.2} \qquad (5)$$

where $\sigma_{sg}(STP,\lambda))$ is the scattering coefficient at standard temperature and pressure for a given wavelength, γ is a factor accounting for molecular anisotropy, T is the temperature in K, and P is the pressure in hPa. All required parameters are most accurately known for dry air and CO_2; thus, these are the calibration gases of choice for most nephelometer applications[16], including our own. For air and CO_2, at 532nm $\sigma_{sg}(STP)$-values are 1.3888×10^{-5} and 3.5969×10^{-5} (m^{-1}), respectively, and γ-values are 0.01442 and 0.04325, respectively.[15,17] Thus, $\beta_{air}(STP)$ is 1.63×10^{-6} (m^{-1} sr^{-1}) and $\beta_{CO2}(STP)$ is 4.12×10^{-6} (m^{-1} sr^{-1}). Given knowledge of the calibration gases, the calibration constants are determined as:

$$k_2 = \frac{(\beta_{CO2} - \beta_{air})}{(C_{CO2} - C_{air})} \qquad C_{wall} = C_{air} - \frac{\beta_{air}}{k_2} \qquad (6)$$

Note that C_{CO2} and C_{air} are actually measured over the angular range 176°-178°, where as the known values, β_{CO2} and β_{air}, are for a 180° scattering angle. Implicit in k_2, then, is the conversion from $\sigma_{gas,176°\text{-}178°}$ to β_{gas}. This conversion is carried over with k_2 to all other scattering measurements.

We have performed a 4-point calibration (using air and CO_2 at pressures of 1 and 0.5 atm) of the 180° nephelometer which indicates excellent linearity (Figure 4) and very small wall scattering. (C_{wall} is less than 5% of C for particle-free air.) In addition, we have performed numerous measurements of air and CO_2 to study noise levels, mechanical stability, sensitivity to laser beam alignment, etc. These tests yielded calibration constants that varied by <4% under normal working conditions and indicated a detection limit for 5-minute averages of approximately 0.10 times β_{air}.

4.0 Relation to previous instruments and approaches

A. The backscattersonde

The "backscattersonde" described by Rosen and Kjome[18] is similar to our 180° nephelometer in that it offers a local measurement of β_p. It is light and inexpensive, and thus well-suited for balloon-borne measurements of atmospheric backscatter versus altitude; in contrast, the instrument described herein is currently both too large and too expensive for routine balloon deployment. The backscattersonde has been used to determine the lidar ratio by running it in parallel with a separate instrument that measures scattering and with assumptions about particle absorption.[19-21]

The backscattersonde has an open sensing volume and a flashlamp light source, so it cannot be calibrated in the laboratory with gases or with particles of known concentration, size and refractive index, and it can only be used at night. The present calibrations rely on measurements of air Rayleigh backscattering in the stratosphere in the winter Arctic polar vortex, where particle concentrations are believed to be insignificant. Previous or subsequent measurements in other regions rely on inter-instrument calibration via comparison to reference instruments. However, optical and electronic components may be subject to drift and the resulting uncertainty has not been determined. The instrument senses backscattering over a broad angular range (~160°-179°) and over two broad wavelength ranges centered at 490 and 700 nm, with bandwidths of about 100 nm. The backscatter at 532 nm is derived by linear interpolation. For these reasons, even for a calibrated system, converting the measured quantity to β_p at 532 nm would require an optical model of the instrument and Mie calculations based on assumptions about particle size, refractive index, and sphericity. Thus, the backscattersonde offers a proxy for β_p at 532nm that requires calculations and assumptions not required by our 180° nephelometer.

B. Raman lidar & High Spectral Resolution Lidar (HSRL)

Another technique related to the one presented herein is the Raman lidar method.[22-29] Molecular and aerosol contributions to light extinction are separated in this method by measuring

Raman-shifted laser light at the appropriate wavelengths for nitrogen, oxygen, carbon dioxide and/or water vapor. Laser light that has been elastically scattered by both molecules and aerosols is also measured. The intensity of the Raman-shifted backscatter from a given altitude depends on $\sigma_{sg}(z)$, $\sigma_{sp}(z)$, and on $\beta_{gas}(z)$, but not on $\beta_p(z)$. The terms $\sigma_{sg}(z)$ and $\beta_{gas}(z)$ can be calculated, given an assumed or measured (with a radiosonde) atmospheric density, so inversion yields $\sigma_{sp}(z)$ at the Raman-shifted wavelength. Aerosol extinction at the original laser wavelength is determined from the Raman-shifted signal by using an assumed wavelength-dependence of light scattering, which is based on an assumed size distribution.

To date, this technique has mostly been applied to ultra-violet wavelengths. Because of the strong wavelength dependence of the lidar ratio (according to Mie calculations) for particles below about 10 μm, lidar ratios measured at UV wavelengths with Raman lidar are not directly applicable to visible-wavelength lidar. Conversion to visible wavelengths requires use of an aerosol model (essentially, an assumed aerosol size distribution) that can introduce uncertainties of a factor of two.

High spectral resolution lidar (HSRL), like Raman lidar, solves the lidar inversion problem by separating the backscattered light into particulate and molecular components.[30-33] HSRL takes advantage of the fact that molecules in the atmosphere have much greater Brownian motion than particles, so backscattered light from molecules is wavelength-broadened around the original laser wavelength. An interferometer is used to measure this broadened molecular backscatter. As with the Raman-shifted backscatter described above, the molecular return signal depends on total extinction and gaseous backscatter only, so $\sigma_{sg}(z)$ can be determined directly, given $\sigma_{sg}(z)$ and $\beta_{gas}(z)$.

Both the Raman lidar and HSRL are quite expensive and technologically complex. Like other remote or open-air devices (including the backscattersonde), they cannot be calibrated with laboratory particles of known optical properties, such that the absolute accuracy of their inversion is difficult to quantify. Independent verification of the measured optical properties is therefore useful. On the other hand, these open-air devices have the enormous advantage of measuring the

undisturbed ambient aerosol and can be used to explore vertical variations in the lidar ratio and its sensitivity to ambient relative humidity.

C. Calibration approaches for lidars with elastic backscatter only

Retrieval of aerosol optical parameters from lidar systems without Raman capability is also possible, given certain assumptions and/or coincident measurements by other instruments. Sunphotometers are often used to measure total column optical depth (τ) for vertically pointing lidars.[34-37] Generally, τ must be wavelength corrected to the given lidar wavelength. In addition, τ is measured for the entire atmosphere, whereas the lidar measurement is only over a portion of the atmosphere (z_L-z in Eqn. 1). One approach is to assume that above z the atmosphere is aerosol-free and use a fixed lidar ratio to determine aerosol extinction from the lidar and sunphotometer data alone.[34] Takamura *et al.*[35,36] used the sunphotometer in conjunction with an optical particle counter (OPC), which determines the ground-level aerosol size distribution for an assumed index of refraction. They calculated aerosol extinction and backscatter - and thus the lidar ratio - from Mie theory and the OPC data. Aerosol optical properties were considered to be horizontally and vertically homogeneous. They assumed the return signal from the stratosphere was aerosol-free and so used it for lidar absolute calibration. As the authors point out, this approach is invalid after significant volcanic eruptions, such as of Mt. Pinatubo in June, 1991.

Hayasaka *et al.*[37] took a similar approach to Takamura *et al.*, but instead of using an OPC they used an aureolemeter, which views forward-scattered sunlight. The instrument gives a columnar averaged size distribution, assuming spherical aerosols with a given index of refraction; this information is useful for Mie calculations of aerosol scattering. An advantage of this method is that forward-scattered radiation is not as sensitive to shape and index of refraction as it is to size, so error in the assumed input parameters is not likely to significantly corrupt the derived size distribution.

Bistatic lidars measure scattered light at a range of angles, providing information on the phase function of the column-averaged aerosol. This data can be used to determine the most probable aerosol index of refraction and size distribution.[38,39] Mie calculations are then

employed to perform the lidar inversion. Hoff *et al.*[12] used a ground-based nephelometer with a vertically-pointing lidar and calculated lidar ratios by assuming no light absorption and vertical homogeneity. Yang *et al.*[40] made no auxiliary measurements, using Mie theory with an assumed aerosol size distribution and refractive indices from D'Almeida *et al.*[41] Lidar ratios calculated from their retrieved data are unrealistically low (2 to 7), leading us to conclude that either their method or the data from D'Almeida *et al.* is erroneous.

Several groups have made measurements of aerosol optical properties in the boundary layer using horizontally pointing lidars.[42-44] This is a somewhat easier retrieval problem, in that assumptions of aerosol homogeneity over the lidar optical path are more likely to be accurate. Jorgensen *et al.*[42] used a hard target with fixed optical properties to calibrate their lidar, then derived aerosol optical properties for a generated smoke cloud of high optical depth. Young *et al.*[43] used meteorological data from the lidar site to calculate molecular scattering and an Active Scattering Aerosol Spectrometer Probe (ASASP) to determine the aerosol size distribution at the site. In horizontally homogeneous conditions (i.e., when the lidar signal decreased linearly with range), the lidar ratio could be derived from this data alone. Zhang and Hu[44] used filter sampling methods and an optical particle counter to determine aerosol size and refractive index, then calculated lidar ratios using Mie theory. Assuming horizontal homogeneity, the system calibration was complete.

All of these approaches to lidar data retrieval require some combination of additional measurements and assumptions about the physical properties of the aerosols. Mie theory is almost always employed to connect these properties to light scattering characteristics, which must be known to retrieve physically meaningful data from the lidar signal. However, Mie theory may inaccurately represent the optical properties of the aerosols, especially if they are non-spherical, even if the input parameters are correct. Direct determination of aerosol's lidar ratio eliminates the need for measurements and assumptions about particle physical properties and subsequent calculation of optical properties.

5.0 Lidar ratio measurements

Field measurements of the lidar ratio, K (Eq. 2) were made at Cheeka Peak Observatory (CPO), located at 480m altitude in the far northwest corner of Washington state. This coastal station samples a wide variety of airmass types, including clean marine air (the dominant category), continental air affected by urban/industrial pollution in the Pacific Northwest, and occasionally, polluted air from Asia. Three optical quantities, σ_{sp}, σ_{ap}, and β_p, were measured to calculate K. The first two, which determine σ_{ep}, were measured with existing instrumentation. Scattering was measured using an integrating nephelometer (TSI model 3563) and σ_{ap} by an absorption photometer that responds to differential transmission of light through a filter (model PSAP, Radiance Research, Seattle, WA.) All quantities were measured at low relative humidity (RH < 40%). Impactors were used to alternate every 5 minutes between measuring aerosol with diameter D=10μm and aerosol with D=1μm, so both fine and coarse mode data were acquired.

Several adjustments to the nephelometer and absorption photometer measurements were necessary for accurate determination of K. We corrected for angular non-idealities in the nephelometer measurement of σ_{sp} using the procedure described by Anderson and Ogren[16]. For the absorption photometer, we used the calibration and scattering correction recommended by Bond et al.[45]. Finally, both scattering and absorption were measured at 550 nm wavelength and were adjusted to the 532 nm laser wavelength using a power law relationship as defined by the ångström exponent, å:

$$\text{å}(\lambda_1/\lambda_2) = -\frac{\log\left(\sigma_{sp}^{\lambda_1}/\sigma_{sp}^{\lambda_2}\right)}{\log(\lambda_1/\lambda_2)} \qquad (7)$$

The value of å was empirically determined for σ_{sp} by using the 3-wavelength nephelometer scattering measurements at 550 and 450 nm. For conversion of σ_{ap} from 550 to 532 nm, å was assumed to be 1.0. The combined effect of these adjustments is to increase light extinction, σ_{ep}, by up to 40% relative to its uncorrected value, primarily due to the correction of the integrating nephelometer for truncation errors for coarse particles[16,45]. Following these adjustments, the uncertainty in σ_{ep} is less than 20% for the Cheeka Peak data set. These corrections are more

important for the coarse particle aerosols (e.g. dust, sea salt) and less important for fine particles (e.g. industrial pollution).

Aerosol optical properties during two distinct sampling periods, one continental and one marine, are presented in Tables 2-4 and Figures 5 & 6. The continental data are separated into two cases (Tables 2 & 3) to reflect a step-change in aerosol light absorption (see Figure 5d). Our measurement protocol involved separate analysis of sub-1 µm and sub-10 µm diameter particles. Here we present only the sub-10 µm measurements; however, analysis of the complete data set reveals that the continental aerosol is dominated by sub-µm particles while the marine aerosol is dominated by super-µm particles. This is confirmed by the contrasting values of å - around two for the continental period (Figure 5e) and zero for the marine period (Figure 6e). The continental aerosol has a significant absorption component, indicative of pollution, whereas the marine aerosol is non-absorbing, consistent with seasalt composition.

The fine-mode dominated continental air has a much higher lidar ratio that the coarse-mode dominated marine air, as is consistent with Mie theory. For the marine case, the lidar ratio is relatively constant, despite large changes in total aerosol amount (as reflected by changes in total extinction, Figure 6b). In all three cases, the variability in the lidar ratio is ~15%, which we attribute to instrumental noise rather than to real variation in the ambient aerosol lidar ratio. The 180° nephelometer laser stability degraded during the field campaign, significantly affecting the instrument performance. The data presented herein are from times when the laser was relatively well-behaved. Clean air measurements were used to correct for offset variation, and span gas calibrations were made in close proximity to each sample period. Based on this information, we estimate that the lidar ratios presented herein are accurate to within 20%. We expect to improve the uncertainty in our measurements when the instrument is run with a laser which conforms to the manufacturer stability specification of <1% variation. Still better results should be possible with higher aerosol loads via higher signal-to-noise ratios.

6.0 Conclusions and future work

The 180° nephelometer presented herein, when used with a total-scatter nephelometer and an instrument that measures light absorption, allows for empirical determination of β_p and the lidar ratio, obviating the need to rely exclusively on values calculated from Mie theory. Such calculations not only involve uncertainties associated with input size distributions and refractive indices but also rely on assumptions of particle homogeneity and sphericity. The instrument is suitable for routine ground-based monitoring as well as periodic airborne surveys of β_p and K. The closed-cell design of the 180° nephelometer permits an absolute calibration with gases; therefore, β_p can be determined without assumptions about particle shape, composition, or state of mixture.

Initial field results show a sharp contrast between the lidar ratio of polluted continental aerosol (60-70) and clean marine aerosol (~20). Uncertainties in these values are on the order of 20%, largely due to instrumental noise in the 180° nephelometer. This noise has been traced to low photon counting rates for the reference beam and to erratic behavior of the laser during the field deployment.

Minor changes to the optical arrangement are being implemented to increase the reference beam intensity. Following the methods described by Anderson et al.[14] for the integrating nephelometer, we will validate the measurement of particulate backscatter using laboratory generated monodisperse latex spheres of known β_p.

Further enhancements to the nephelometer could be undertaken. The current design allows for measurement of both β_p and σ_{sp} with a single instrument, via manual switching between the laser and nephelometer lamp light sources. However, shutters synchronized with the reference beam chopper could be placed in front of the laser and the lamp, allowing nearly simultaneous measurement of the two quantities, β_p and σ_{sp}.

Shape effects may be a dominant source of uncertainty in theoretical determinations of the lidar ratio, especially for coarse mode dust and seasalt particles. Our empirical method of determining the lidar ratio could be used to study shape effects and would be enhanced in this

regard by adding a polarization measurement. At present, the instrument measures the sum of polarized plus depolarized scattered light. A second detection channel could be added to measure only the depolarized scattered light. The ratio of these two quantities (the depolarization ratio) should be a sensitive indicator of non-sphericity. Modifications to this end are being pursued.

Acknowledgments: This work was supported by the National Aeronautics and Space Administration (grant #NAG 1 1877) with additional support provided by the National Science Foundation (grant #ATM-9320871), and by the National Oceanic and Atmospheric Administration (Joint Institute for the Study of the Atmosphere and Ocean (JISAO) agreement #NA37RJ0198, contribution #575). We would also like to thank Steven Domonkos of the University of Washington Dept. of Atmospheric Sciences for his invaluable contributions to the deign and construction of the instrument.

References and Notes

1. J. H. Seinfeld, R. J. Charlson, P. A. Durkee, D. Hegg, B. J. Huebert, J. Kiehl, M. P. McCormick, J. A. Ogren, J. E. Penner, V. Ramaswamy, and W. G. Slinn, Aerosol Radiative Forcing and Climate Change, Washington, D. C., National Research Council, National Academy Press, pp. 161 (1996).

2. Instrument calibration relates detected photon counts to backscatter. Lidar calibration depends on factors such as pulse strength, detector gain, and system geometry -- see Ref. 12.

3. The lidar ratio is defined herein such that $K = \frac{8\pi}{3}$ for Rayleigh scattering.

4. M. P. McCormick, D. M. Winker, E. V. Browell, J. A. Coakley, C. S. Gardner, R. M. Hoff, G. S. Kent., S. H. Melfi, R. T. Menzies, C. M. R. Platt, D. A. Randall, and J. A. Reagan, "Scientific investigations planned for the lidar in-space technology experiment (LITE)", Bull. Amer. Meteo. Soc. **74,** 205-214 (1993).

5. B. E. Anderson, W. B. Grant, G. L. Gregory, E. V. Browell, J. E. Collins, G. W. Sachse, D. R. Bagwell, C. H. Hudgins, D. R. Blake, N. J. and Blake, "Aerosols from biomass burning over the tropical South Atlantic region: Distributions and impacts", J. Geophys. Res. **101,** 24117-24137 (1996).

6. E. V. Browell, C. F. Butler, S. A. Kooi, M. A. Fenn, R. C. Harriss, and G. L. Gregory, "Large-scale variability of ozone and aerosols in the summertime Arctic and Sub-Arctic troposphere", J. Geophys. Res. **97,** 16433-16450 (1992).

7. E. V. Browell, M. A. Fenn, C. F. Butler, W. B. Grant, R. C. Harriss, and M. C. Shipham, "Ozone and aerosol distributions in the summertime troposphere over Canada", J. Geophys. Res. **99,** 1739-1755 (1994).

8. E. V. Browell, G. L. Gregory, R. C. Harriss, and V. W. J. H. Kirchhoff, "Ozone and aerosol distributions over the Amazon Basin during the wet season", J. Geophys. Res. **95,** 16887-16901 (1990).

9. B. T. N. Evans, "Sensitivity of the backscatter/extinction ratio to changes in aerosol properties: implications for lidar", Appl. Opt. **27,** 3299-3305 (1988).

10. S. A. Kwon, Y. Iwasaka, T. Shibata, and T. Sakai, "Vertical distribution of atmospheric particles and water vapor densities in the free troposphere: lidar measurement in spring and summer in Nagoya, Japan", Atmos. Environ. **31,** 1459-1465 (1997).

11. P. B. Russell and B. M. Morley, "Orbiting lidar simulations. 2: Density, temperature, aerosol, and cloud measurements by a wavelength-combining technique", Appl. Opt. **21,** 1554-1563 (1982).

12. R. M. Hoff, L. Guise-Bagley, R. M. Staebler, H. A. Wiebe, J. Brook, B. Georgi, & T. Dusterdiek, "Lidar, nephelometer, and in situ aerosol experiments in southern Ontario". J. Geophys. Res., **101**(D14), 19,199-19,209, (1996).

13. T. L. Anderson, D. S. Covert, S. F. Marshall, M. L. Laucks, R. J. Charlson, A. P. Waggoner, J. A. Ogren, R. Caldow, R. Holm, F. Quant, G. Sem, A. Wiedensohler, N. A. Ahlquist, and

T. S. Bates, "Performance characteristics of a high-sensitivity, three-wavelength, total scatter/backscatter nephelometer", J. Atmos. Oceanic Technol. **13,** 967-986 (1996).

14. Chandrasekhar, S. Radiative Transfer. New York: Dover (1960).

15. A. Bucholtz, "Rayleigh-scattering calculations for the terrestrial atmosphere", Appl. Opt. **34,** 2765-2773 (1995).

16. T. L. Anderson and J. A. and Ogren, "Determining aerosol radiative properties using the TSI 3563 integrating nephelometer", Aerosol Sci. Technol., in press (1998).

17. A. T. Young, "Revised depolarization corrections for atmospheric extinction", Appl. Opt. **19,** 3427-3428 (1980).

18. J. M. Rosen, and N. T. Kjome, "Backscattersonde: a new instrument for atmospheric aerosol research", Appl. Opt. **30,** 1552-1561 (1991).

19. J. M. Rosen, R. G. Pinnick, and D. M. Garvey, "Measurement of extinction-to-backscatter ratio for near-surface aerosols", J. Geophys. Res. **102,** 6017-6024 (1997).

20. J. M. Rosen, T. Kjome, and J. B. Liley, "Tropospheric aerosol backscatter at a midlatitude site in the northern and southern hemispheres", J. Geophys. Res. **102,** 21329-21339 (1997).

21. J. M. Rosen, & T. N. Kjome, "Balloon-borne measurements of the aerosol extinction-to-backscatter ratio". J. Geophys. Res., **102**(D10), 11,165-11,169, (1997).

22. A. Ansmann, M. Riebesell, and C. Weitkamp, "Measurement of atmospheric aerosol extinction profiles with a Raman lidar", Appl. Phys. B **55,** 18-28 (1992).

23. A. Ansmann, M. Riebesell, U. Wandinger, C. Weitkamp, E. Voss, W. Lahmann, and W. Michaelis, "Combined Raman elastic-backscatter LIDAR for vertical profiling of moisture, aerosol extinction, backscatter, and LIDAR ratio", Optics Lett. **15**(13), 746-748 (1990).

24. A. Ansmann, U. Wandinger, M. Riebesell, C. Weitkamp, and W. Michaelis, "Independent measurement of extinction and backscatter profiles in cirrus clouds by using a combined Raman elastic-backscatter lidar", Appl. Opt. **31,** 7113-7131 (1992).

25. A. Ansmann, I. Mattis, U. Wandinger, and F. Wagner, "Evolution of the Pinatubo Aerosol: Raman Lidar Observations of Particle Optical Depth, Effective Radius, Mass and Surface Area over Center Europe at 53.4°N", J. Atmos. Sci. **54,** 2630-2641 (1997).

26. D. Muller, U. Wandinger, D. Althausen, I. Mattis, & A. Ansmann, "Retrieval of physical particle properties from lidar observations of extinction and backscatter at multiple wavelengths". Appl. Opt., **37**(12), 2260-2263, (1998).

27. P. von der Gathen, "Aerosol extinction and backscatter profiles by means of a multiwavelength Raman lidar: a new method without *a priori* assumptions". Appl. Opt., **34**(3), 463-466, (1995).

28. R. A. Ferrare, S. H. Melfi, D. N. Whiteman, K. D. Evans, and R. Leifer, "Raman lidar measurements of aerosol extinction and backscattering: 1. Methods and comparisons". J. Geophys. Res., **103**(D16), 19,663-19,672, (1998).

29. R. A. Ferrare, S. H. Melfi, D. N. Whiteman, K. D. Evans, M. Poellot, and Y. J. Kaufman, "Raman lidar measurements of aerosol extinction and backscattering: 2. Derivation of aerosol real refractive index, single-scattering albedo, and humidification factor using Raman lidar and aircraft size distribution measurements". J. Geophys. Res., **103**(D16), 19,673-19,689, (1998).

30. S. T. Shipley, D. H. Tracy, E. W. Eloranta, J. T. Trauger, J. T. Sroga, F. L. Roesler, and J. A. Weinman, "High spectral resolution lidar to measure optical scattering properties of atmospheric aerosols. 1: Theory and instrumentation". Appl. Opt., **22**(23), 3716-3724, (1983).

31. J. T. Sroga, E. W. Eloranta, S. T. Shipley, F. L. Roesler, and P. J. Tryon, "High spectral resolution lidar to measure optical scattering properties of atmospheric aerosols. 2: Calibration and data analysis". Appl. Opt., **22**(23), 3725-3732, (1983).

32. C. J. Grund and E. W. Eloranta, "University of Wisconsin high spectral resolution lidar". Opt. Eng., **30**(1), 6-12, (1991).

33. P. Piironen and E. W. Eloranta, "Demonstration of a high-spectral-resolution lidar based on an iodine absorption filter". Opt. Lett., **19**(3), 234-236, (1994).

34. T. Murayama, M. Furushima, A. Oda, & N. Iwasaka, (1997). Aerosol optical properties in the urban mixing layer studies by polarization lidar with meteorological data. In A. Ansmann, R. Neuber, P. Rairoux, & U. Wandinger (Eds.), Advances in Atmospheric Remote Sensing with Lidar (pp. 19-22). Springer-Verlag.

35. T. Takamura, & Y. Sasano, "Aerosol optical properties inferred from simultaneous lidar, aerosol-counter and sunphotometer measurements". J. Met. Soc. Japan, **68**(6), 731-739, (1990).

36. T. Takamura, Y. Sasano, & T. Hayasaka, "Tropospheric aerosol optical properties derived from lidar, sun photometer, and optical particle counter measurements". Appl. Opt., **33**(30), 7132-7140, (1994).

37. T. Hayasaka, Y. Meguro, Y. Sasano, & T. Takamura, "Stratification and size distribution of aerosols retrieved from simultaneous measurements with lidar, a sunphotometer, and an aureolemeter". Appl. Opt., **37**(6), 961-970, (1998).

38. H. Yoshiyama, A. Ohi, & K. Ohta, "Derivation of the aerosol size distribution from a bistatic system of a muliwavelength laser with the singular value decomposition method.". Appl. Opt., **35**(15), 2642-2648, (1996).

39. G. Pandithurai, P. C. S. Devara, P. Ernest Raj, & S. Sharma, "Aerosol size distribution and refractive index from bistatic lidar angular scattering measurements in the surface layer". Remote Sens. Environ., **56**, 87-96, (1996).

40. S. Yang, W. Cotton, & T. Jensen, "Feasibility of retrieving aerosol concentration in the atmospheric boundary layer using multitime lidar returns and visual range". J. Atm. and Ocean. Tech., **14**, 1064-1078, (1997).

41. G. A. D'Almeida, P. Koepke, & E. P. Shettle, Atmospheric Aerosols: Global Climatology and Radiative Characteristics. Deepak (1991).

42. H. E. Jorgensen, T. Mikkelsen, J. Streicher, H. Herrmann, C. Werner, & E. Lyck, "Lidar calibration experiments". Appl. Phys. B, **64**, 355-361, (1997).

43. S. A. Young, D. R. Cutten, M. J. Lynch, & J. E. Davies, "Lidar-derived variations in the backscatter-to-extinction ratio in Southern Hemisphere coastal maritime aerosols". Atmos. Environ., **27A**, 1541-1551, (1993).

44. J. Zhang, & H. Huanling, "Lidar calibration: a new method". Appl. Opt., **36**(6), 1235-1238, (1997).

45. T. Bond, R. J. Charlson, and J. Heintzenberg, "Quantifying the emission of light-absorbing particles: Measurements tailored to climate studies", Geophys. Res. Lett., **25**(3)**,** 337-340, (1998).

TABLE 1. Sensitivity of aerosol optical depth to lidar ratio. Calculations using aerosol layers detected at night over Africa during the LITE Mission. (Calculations by Mark Vaughan, NASA Langley.)

	Case 1†		Case 2‡	
K	τ_p	$?\log\tau_p / ?\log K$	τ_p	$?\log\tau_p / ?\log K$
10	0.022	1.06	0.021	1.09
20	0.048	1.14	0.046	1.20
30	0.077	1.22	0.077	1.33
40	0.111	1.31	0.115	1.46
50	0.150	1.42	0.162	1.63
60	0.196	1.55	0.221	1.83
70	0.252	1.71	0.299	2.09
80	0.321	1.91	0.404	2.47
90	0.408	2.18	0.558	3.10
100	0.523	2.55	0.817	4.25

†Case 1: Average over 400 records beginning MET 009/01:09:02.60. Aerosol layer extends from 1388 to 5013 m above sea level.

‡Case 2: Average over 300 records beginning MET 009/01:10:32.60. Aerosol layer extends from 1532 to 5832 m above sea level.

TABLE 2. Aerosol optical properties at 532 nm measured at Cheeka Peak Observatory, Washington State, Spring, 1998, Case 1: Continental sampling from day 64.15 to 64.68.

Statistical Parameter	σ_{sp} (Mm^{-1})	σ_{ap} (Mm^{-1})	β ($Mm^{-1}\ sr^{-1}$)	K (sr)
average	15.73	1.59	0.29	60.4
stan. dev.	1.04	0.15	0.04	7.6
rel. stan. dev.	7%	9%	15%	13%

$Mm^{-1} = 10^6\ m^{-1}$.

TABLE 3. As in Table 2 except Case 2: Continental sampling from day 64.78 to 65.00.

Statistical Parameter	σ_{sp} (Mm^{-1})	σ_{ap} (Mm^{-1})	β (Mm^{-1} sr^{-1})	K (sr)
average	15.28	2.07	0.25	69.9
stan. dev.	1.65	0.31	0.04	9.7
rel. stan. dev.	11%	15%	16%	14%

$Mm^{-1} = 10^6\ m^{-1}$.

TABLE 4. As in Table 2 except Case 3: Marine sampling from day 75.25 to 75.95.

Statistical Parameter	σ_{sp} (Mm^{-1})	σ_{ap} (Mm^{-1})	β (Mm^{-1} sr^{-1})	K (sr)
average	9.83	0.04	0.48	21.1
stan. dev.	1.85	0.05	0.12	3.7
rel. stan. dev.	19%	-	25%	17%

$Mm^{-1} = 10^6\ m^{-1}$.

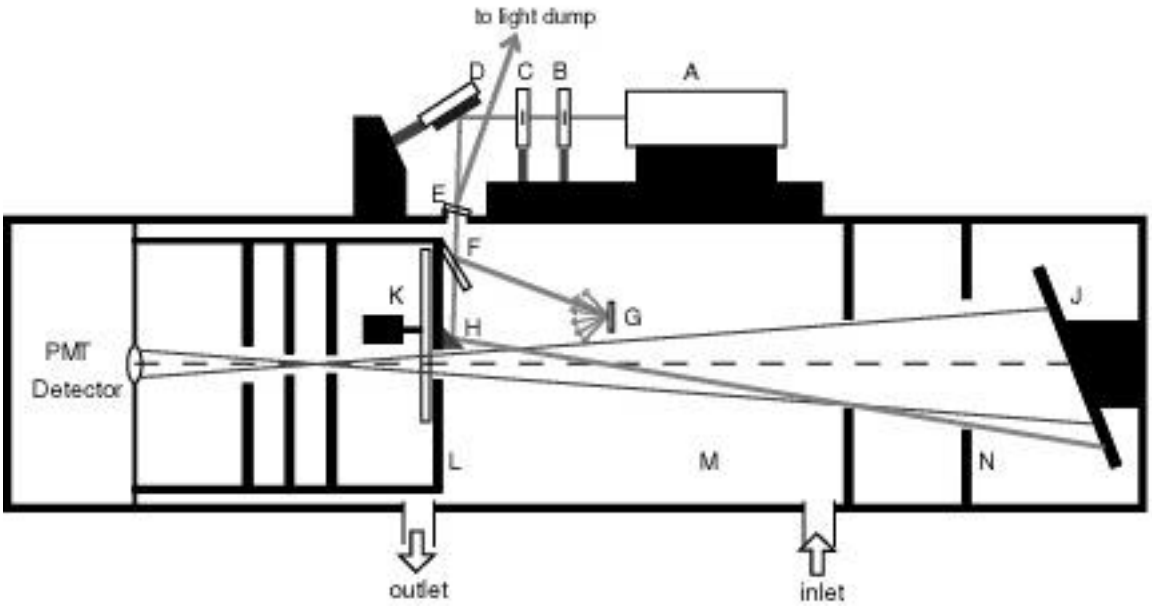

FIGURE 1: Design of the 180° backscatter nephelometer (vertical scale greatly exaggerated.) A laser light source (A) produces a beam with a $1/e^2$ diameter of 0.6mm. The beam is spatially filtered (B & C) through a pair of apertures and folded (D) into the nephelometer cavity through an anti-reflection coated window (E). The beam enters the nephelometer perpendicular to the view volume optical axis at the baffle (L) housing the nephelometer reference chopper (K). This baffle establishes one end of the scattering volume. A coated glass window (F) mounted on the baffle reflects ~1% of the laser light up to G (see Figure 2) for use as a reference beam. A small prism with a mirror coating on the hypotenuse and flat black coating on all other sides (H) folds the remaining 99% of the beam at a 2.5° angle to the nephelometer optical axis (dashed line). The prism size was minimized so that the beam could be folded as close to the detector field of view as possible. The angular field of view of the detector is 1.0°. The intersection of the light source with this field of view defines the sensing volume. With the present geometry, light scattered within the sensing volume at angles between 176.4° and 178.4° is detected. The laser beam leaves the detector field of view at baffle M, restricting the sensing volume to the region between the aerosol inlet and outlet. The beam terminates at a light dump (J). Baffles M and N shield any light reflected off the black glass light dump from reaching the detectors. All surfaces inside the nephelometer, other than active optical surfaces, are coated with black optical paint to minimize stray light scatter.

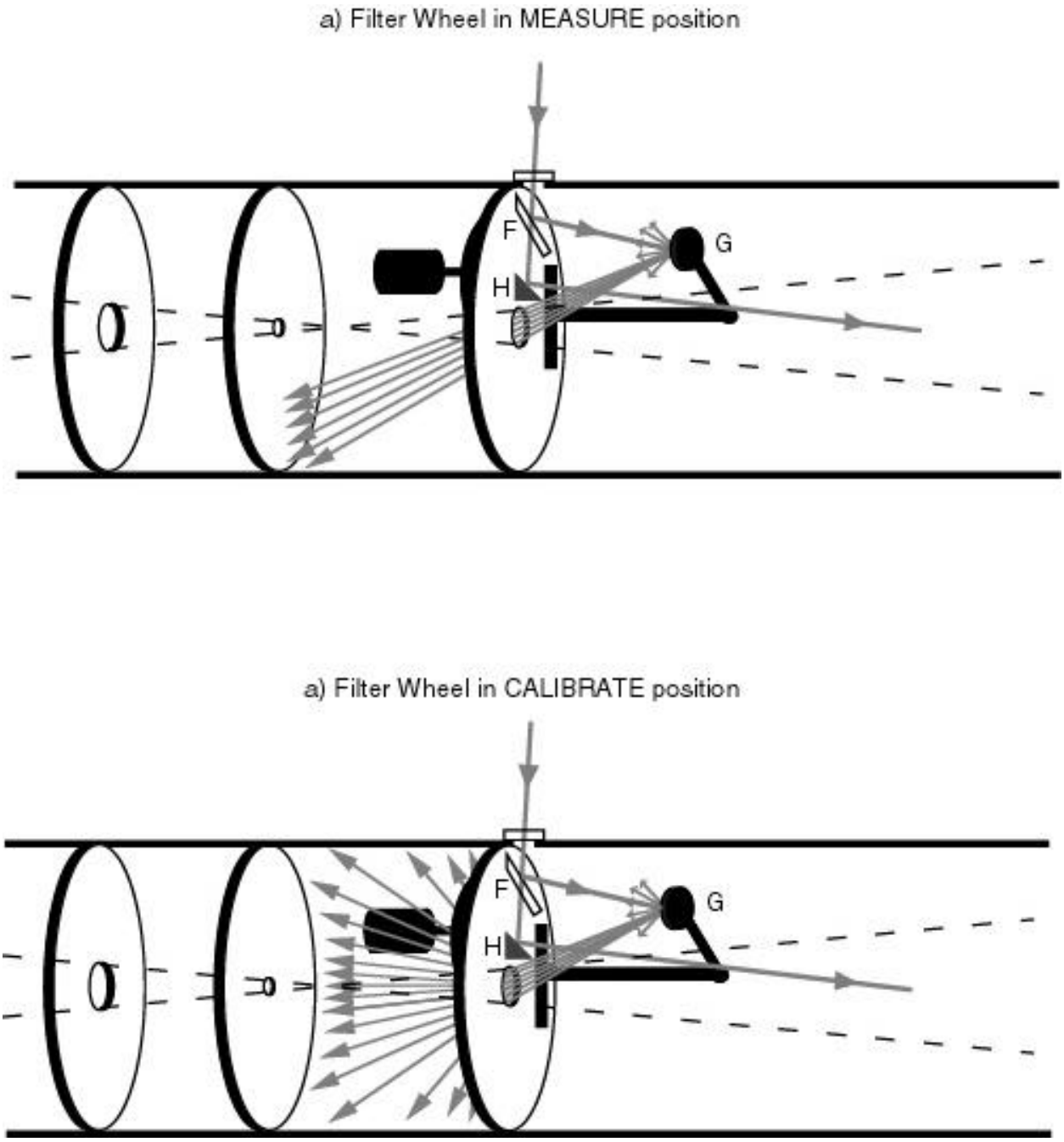

FIGURE 2: Variations in the laser intensity and photomultiplier tube (PMT) sensitivity are accounted for by continuously monitoring the intensity of a calibration reference beam. As noted above, ~1% of the beam entering the nephelometer volume is split off with an anti-reflection coated window (F) and forms the reference beam. The reference beam is directed at a white disk (G), creating a diffuse light source. The disk is located outside the detector field of view such that the diffusely scattered light does not directly reach the detector when the reference chopper is

in the open (measure) position. (a). The diffuse light strikes baffles and walls coated with black optical paint, and is largely absorbed. When the reference chopper is in the "calibrate" position, some of the diffuse light strikes a neutral-density coated glass surface, transmitting some of the light to the detector (b). Variations in laser intensity are manifested as changes in the "calibrate" photon counts, C_{cal}, which are used to calculate the system signal as described in the text.

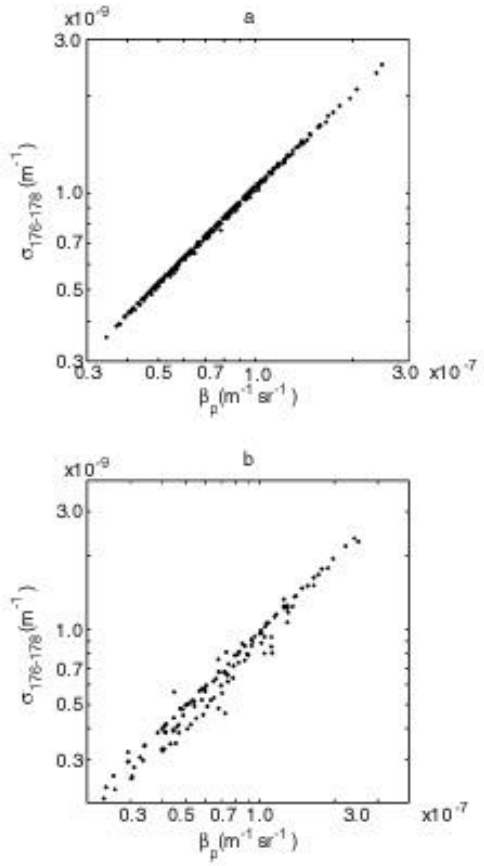

FIGURE 3: The scattering integral of 176° to 178° measured by the 180° nephelometer is an excellent proxy for 180° backscatter. Accuracies are ±2% for the accumulation mode and ±10% for the coarse mode based on Mie calculations for lognormal particle size distributions as shown above. Test cases used geometric standard deviations ranging from 1.6 to 2.2 and real refractive indices ranging from 1.36 to 1.52. For the accumulation mode (a), volume mean diameter, D_{gv}, ranged from 0.2 to 0.6 μm and single scattering albedo, ω_0, ranged from 0.77 to 1.0. For the coarse mode (b), D_{gv} ranged from 1.0 to 5.0 and ω_0 from 0.85 to 1.0 to represent mass dominated by seasalt or mineral dust.

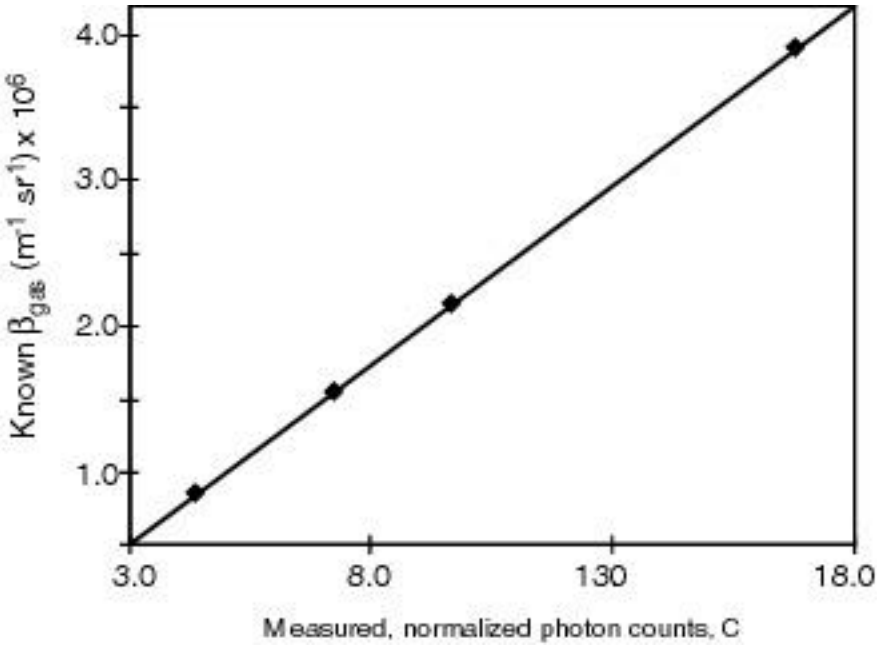

FIGURE 4: Gas calibration results for a "four-point" calibration of the 180° nephelometer. Two measurements were made at 0.5 atm and one at 1.0 atm for both air and CO_2.

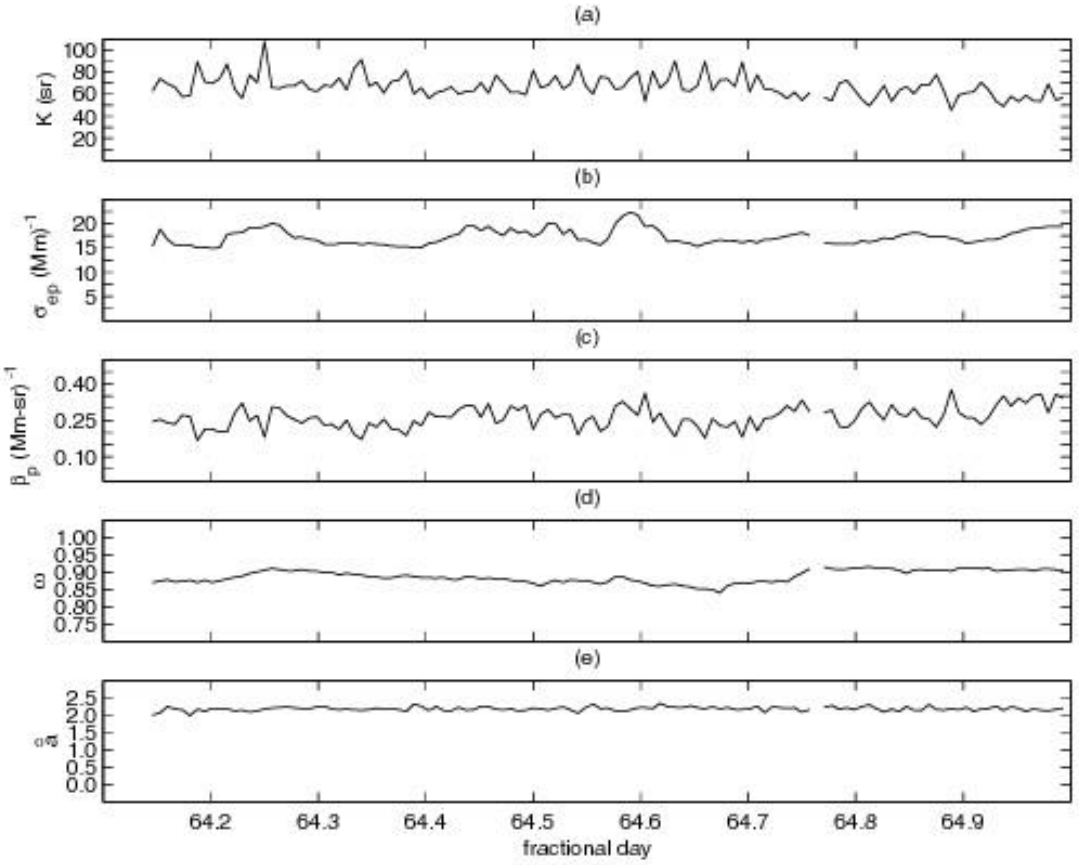

FIGURE 5: Optical properties of continental aerosol measured on March 5, 1998 GMT (day 64) at Cheeka Peak Observatory, Washington.

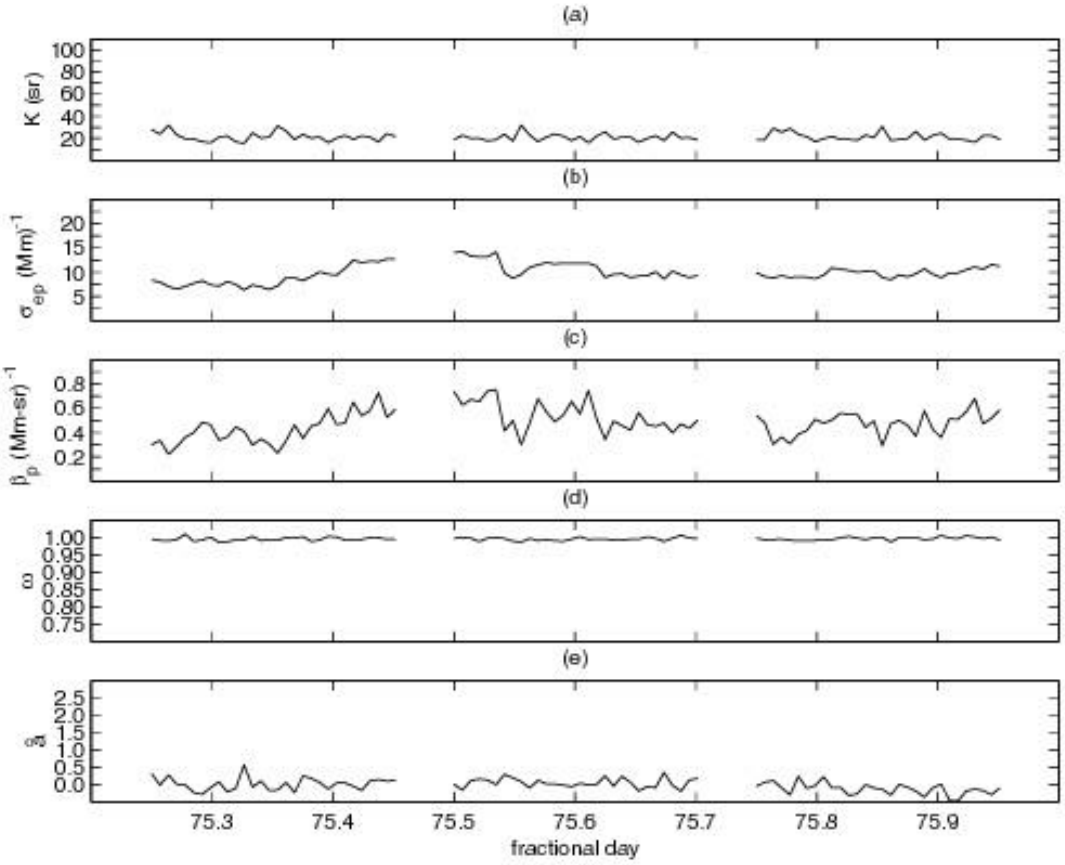

FIGURE 6: Optical properties of marine aerosol measured on March 16, 1998 GMT (day 75) at Cheeka Peak Observatory, Washington.